Fluctuation-Induced Phenomena in Nanoscale Systems: Harnessing the Power of Noise

M. T. Homer Reid, Alejandro W. Rodriguez, and Steven G. Johnson

(Invited Paper)

Abstract—The famous Johnson-Nyquist formula relating noise current to conductance has a microscopic generalization relating noise current *density* to microscopic *conductivity*, with corollary relations governing noise in the components of the electromagnetic fields. These relations, known collectively in physics as *fluctuation–dissipation* relations, form the basis of the modern understanding of *fluctuation-induced phenomena*, a field of burgeoning importance in experimental physics and nanotechnology. In this review, we survey recent progress in computational techniques for modeling fluctuation-induced phenomena, focusing on two cases of particular interest: *near-field radiative heat transfer* and *Casimir forces*. In each case we review the basic physics of the phenomenon, discuss semi-analytical and numerical algorithms for theoretical analysis, and present recent predictions for novel phenomena in complex material and geometric configurations.

Index Terms—Johnson, Nyquist, noise, fluctuation, radiation, heat transfer, Casimir effect, finite-difference, boundary-element, modeling, simulation, CAD

I. INTRODUCTION

EVERY electrical engineer knows the famous Johnson-Nyquist formula for the noise current through a resistor,

$$\langle I^2 \rangle = 4kTG\Delta f \tag{1}$$

where $\langle I^2 \rangle$ is the mean-square noise current (Fig. 1**a**), kT is the temperature in energy units, $G = 1/R$ is the conductance of the resistor, and Δf is the measurement bandwidth. Equation (1)—which allows designers to quantify, and thus compensate for, the unavoidable presence of noise in physical circuits—is a crucial tool in the circuit designer's kit and a mainstay of the electrical engineering curriculum from its earliest stages [1].

Perhaps less well-known in the EE community is that equation (1) is only one manifestation of a profound and far-reaching principle of physics—the *fluctuation-dissipation theorem*—that relates the mean-square values of various fluctuating quantities to certain physical parameters (known as *generalized susceptibilities*) associated with the underlying system. In equation (1), the fluctuating quantity is the noise current through the resistor, and the generalized susceptibility is the conductance; more generally, as we will see below, the fluctuation–dissipation concept allows us to quantify fluctuations not only in macroscopic device currents but also in

M. T. Homer Reid is with the Research Laboratory of Electronics, Massachusetts Institute of Technology.

Alejandro W. Rodriguez is with the School of Engineering and Applied Sciences, Harvard University, and the Department of Mathematics, Massachusetts Institute of Technology.

S. G. Johnson is with the Department of Mathematics, Massachusetts Institute of Technology.

microscopic current *densities*, from which it is a short step to obtain fluctuations in the components of the electric and magnetic *fields* inside and outside material bodies (Fig. 1**b**). In this case, we will see that the key tools turn out to be nothing but the familiar *dyadic Green's functions*, which describe the electromagnetic fields of prescribed current sources and are computable by any number of standard methods of classical electromagnetism. It is remarkable that many problems in the field of fluctuation-induced phenomena, which would at first blush seem to necessitate complex statistical-mechanical and quantum-mechanical reasoning, in fact reduce in practice to applications of classical electromagnetic theory that would be familiar to any electrical engineer.

But why would we *want* to quantify noise in the individual components of the electromagnetic fields around material bodies? The answer is that these microscopic field fluctuations can mediate *macroscopic* transfers of energy or momentum among the bodies, which become especially dramatic for bodies at submicron separations. In the former phenomenon—*near-field radiative heat transfer*—fluctuating fields in micron-scale gaps between inequal-temperature bodies can lead to a rate of heat transfer between the bodies that can drastically exceed the rate observed at larger separations [2]. In the latter phenomenon—the *Casimir effect*—fluctuating fields around bodies give rise to attractive and repulsive forces between the bodies, which generalize the familiar van der Waals interactions between molecules [3]. Both phenomena become negligibly small for bodies separated by distances of more than a few microns, which places their observation squarely within the domain of
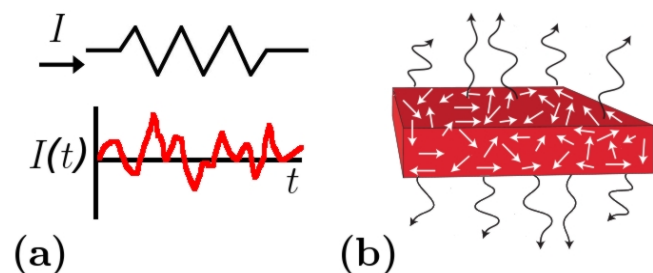

Fig. 1. From macroscopic to microscopic noise. (**a**) The current through a resistor exhibits thermal noise with mean-square amplitude proportional to the conductance [the Johnson-Nyquist formula, equation (1)]. (**b**) More generally, the *microscopic* current density inside a slab of conducting material exhibits fluctuations with mean-square amplitude proportional to the microscopic conductivity [the fluctuation-dissipation theorem, equation (2)]. Knowledge of these microscopic current fluctuations, together with the dyadic Green's functions of the system, allow us to predict the mean-square fluctuations in the components of the electromagnetic fields in space [equations (7) and (12)].

Casimir Effect

Parallel plates [4]	One sphere [5]	Multilayer films [6-7]	Corrugated plates [8]	Two spheres [9]	Crossed cylinders [10]	Needle/aperture [11]
1940s--50s	1960s	1970s--90s	2004	2007	2009	2011

Near-Field Radiative Transfer

Parallel plates [12-13]

Two spheres [14]

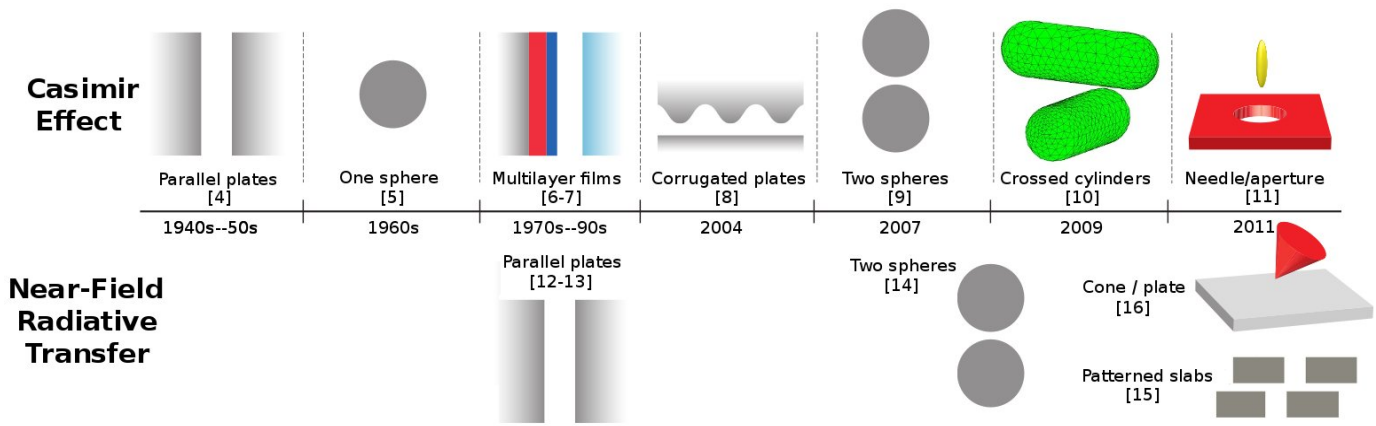Cone / plate [16]

Patterned slabs [15]

Fig. 2. A selective timeline indicating the most complex geometries for which rigorous calculations of Casimir interactions (upper) or near-field radiative heat transfer (lower) were possible at various historical epochs. Note that computational techniques such as finite-difference grids and boundary-element discretization, which have been used in electrical engineering for decades, have only been introduced to the study of fluctuation-induced phenomena within the past five years.

nanoscale physics and engineering.

Although the study of electromagnetic field fluctuations has been an active area of physics for decades, its relevance to electrical engineering was limited for most of that time to equation (1) and other relations quantifying noise in circuits. In the past fifteen years, however, this situation has begun to change; advances in fabrication and measurement technology have ushered in a golden age of experimental studies of fluctuation-induced phenomena [2], [17], and there is reason to believe that this fledgling field of experimental physics will soon become relevant to electrical engineering in areas such as thermal lithography and MEMS technology. This experimental progress has created a demand for modeling and simulation tools capable of predicting fluctuation phenomena in realistic experimental configurations, including the complex, asymmetric geometries and imperfect materials present in real-world systems.

The evolution of theoretical tools for modeling fluctuation-induced phenomena mirrors the historical development of techniques for solving classical electromagnetic scattering problems. In the latter case, the earliest calculations were restricted to highly symmetric geometries (such as Mie's 1908 treatment of scattering from spheres) for which a convenient choice of coordinates and special-function solutions of Maxwell's equations allow the problem to be solved analytically (or at least *semi-analytically*—that is, with results obtained as expansions in special functions, which in practice are then evaluated numerically [18]). Later, fully numerical techniques capable of handling more general geometries gradually became available, including the finite-difference, finite-element, and boundary-element methods introduced in the 1960s, and today the problem of electromagnetic scattering is addressed by a wealth of comprehensive off-the-shelf CAD tools capable of handling extremely complex material and geometric configurations.

Advances in the modeling of near-field radiative transfer and Casimir phenomena have proceeded in similar order (Fig. 2). In both cases the first calculations were restricted to the simplest parallel-plate geometries [4], [12], [13]; these were later extended to other simple shapes such as cylinders [8] and spheres [5], [9], [14], [19]–[21], and, more recently, tools for general geometries have become available [22]–[24]. All of these developments, however, have lagged their antecedents in the classical-scattering domain by many decades; indeed, even for the relatively simple case of two interacting spheres, the Casimir force was only calculated in 2007 [9] and the near-field radiative transfer only in 2008 [14]. One reason for this lag is the relative paucity of experimental data, which—as noted above—are significantly more difficult to gather for fluctuation-induced phenomena than for classical scattering. But perhaps the main reason that practical computations of fluctuation-induced phenomena have been so long in coming is simply that the problems present extraordinary computational challenges. Indeed, as we will see below, calculations of near-field radiative-transfer and Casimir phenomena may be reduced in practice to the solution of classical scattering problems—but a great *number*, thousands or even millions, of separate scattering problems must be solved to compute the heat transfer or Casimir force for a single geometric configuration.

As a result, algorithms for predicting fluctuation phenomena tend to start with techniques familiar to electrical engineers—including the T-matrix, finite-difference, and boundary-element methods of computational electromagnetism—but then proceed to combine and modify these techniques in novel ways to obtain computational procedures that can run in a reasonable length of time. The goal of this review is to describe these computational techniques—and some of the results that they have predicted—in ways that will make sense to electrical engineers.

II. FLUCTUATIONS IN ELECTROMAGNETIC SOURCES AND FIELDS: THE JOHNSON–NYQUIST LAW AND BEYOND

The microscopic generalization of equation (1) is [13], [25]

$$\left\langle J_i(\omega, \mathbf{x}) J_j^*(\omega, \mathbf{x}') \right\rangle$$
$$= \frac{1}{\pi} \delta_{ij} \delta(\mathbf{x} - \mathbf{x}') \left[\frac{\hbar\omega}{2} \coth\left(\frac{\hbar\omega}{2kT} \right) \right] \sigma(\omega, \mathbf{x}) \quad (2)$$

where $J_i(\omega, \mathbf{x})$ is the ith cartesian component of the microscopic current density at position $\mathbf{x}$ and frequency ω, $\hbar$ is Planck's constant, and $\sigma(\omega, \mathbf{x})$ is the position- and frequency-dependent conductivity. [σ is related to the imaginary part of the dielectric permittivity according to $\sigma(\omega, \mathbf{x}) = \omega \cdot \text{Im} \, \epsilon(\omega, \mathbf{x})$; here and throughout we assume that ϵ is linear and isotropic.] In signal-processing language familiar to electrical engineers, the right-hand side of equation (2) is the power spectral density (PSD) of a *colored-noise* process; the fact that the PSD is frequency-dependent (i.e. the fact that this is "colored" instead of white noise) corresponds, in the time domain, to the nonvanishing of correlations between currents at nearby time points.

The similarity between equations (1) and (2) is obvious: on the left-hand side we have a mean product of currents, while on the right-hand side we have a temperature-dependent factor and a measure of conductivity. However, the microscopic equation (2) extends the macroscopic equation (1) in two important ways.

First, whereas equation (1) is a low-frequency, high-temperature approximation that neglects quantum-mechanical effects, equation (2) remains valid at all temperatures and frequencies and explicitly *includes* quantum-mechanical effects. Indeed, taking the low-temperature limit of the bracketed factor in (2), we find

$$\lim_{T \to 0} \left[\frac{\hbar\omega}{2} \coth\left(\frac{\hbar\omega}{2kT} \right) \right] = \frac{\hbar\omega}{2} \quad (3a)$$

and equation (2) thus predicts non-zero current fluctuations even at zero temperature: the well-known quantum-mechanical *zero-point fluctuations*. In the high-temperature limit, on the other hand, we have

$$\lim_{T \to \infty} \left[\frac{\hbar\omega}{2} \coth\left(\frac{\hbar\omega}{2kT} \right) \right] = kT; \quad (3b)$$

this is the *classical* regime, in which all dependence on $\hbar$ is lost and we recover the simple linear temperature dependence of (1). The classical regime is defined by the condition

$$T \gg \frac{\hbar\omega}{2k} \quad \text{or} \quad T \text{ in kelvin} \gg \frac{\omega}{4 \cdot 10^{12} \text{ rad/s}}, \quad (4)$$

a requirement that in practice is always satisfied in circuit-design problems, but which may be readily violated for infrared and optical frequencies ($\omega > 10^{15}$ rad/sec).

The second way in which equation (2) extends the reach of the Johnson-Nyquist result is that, whereas (1) describes only macroscopic currents, (2) gives information on the *microscopic* current density, which in turn can be used to predict fluctuations in the components of the electric and magnetic fields. The relevant tools for this purpose are the *dyadic Green's functions* (DGFs), well-known to electrical engineers from problems ranging from radar and antenna design to microwave device modeling [18]. To recall the definition of these quantities, suppose we have a material configuration characterized by spatially-varying linear permittivity and permeability functions $\{\epsilon(\omega, \mathbf{x}), \mu(\omega, \mathbf{x})\}$. (In most of the problems we consider, ϵ and μ will be piecewise constant in space.) Then the electric DGF describes the field due to a point source in the presence of the material configuration:

$$G_{ij}^{\text{E}}\big(\epsilon, \mu; \omega; \mathbf{x}, \mathbf{x}'\big)$$
$$= \begin{pmatrix} i\text{-component of electric field at } \mathbf{x} \text{ due to} \\ \text{a } j\text{-directed point current source at } \mathbf{x}' \end{pmatrix} \quad (5)$$

while the magnetic DGF G^{M} similarly gives the magnetic field of a point current source. (Here and throughout, all fields and currents are understood to have time dependence $\sim e^{-i\omega t}$.) In (5) we have indicated the dependence of G on the spatially-varying material properties ϵ and μ; the DGFs for a given material configuration can be computed using standard techniques in computational electromagnetism, after which the fields at arbitrary points in space due to a prescribed current distribution may be computed according to

$$E_i(\omega, \mathbf{x}) = \int G_{ij}^{\text{E}}(\omega; \mathbf{x}, \mathbf{x}') J_j(\omega, \mathbf{x}') d\mathbf{x}' \quad (6a)$$

$$H_i(\omega, \mathbf{x}) = \int G_{ij}^{\text{M}}(\omega; \mathbf{x}, \mathbf{x}') J_j(\omega, \mathbf{x}') d\mathbf{x}'. \quad (6b)$$

Note that the long-range nature of the G dyadics ensures that the fields are nonvanishing even at points $\mathbf{x}$ in empty space, i.e. points at which there are no currents or materials.

Armed with equations (2) and (6), we can now make predictions for noise in the components of the electromagnetic fields. For example, the mean Poynting flux at a point $\mathbf{x}$ is a sum of terms of the form (with ω arguments to E, G, and J suppressed)

$$\left\langle E_i(\mathbf{x}) H_j^*(\mathbf{x}) \right\rangle$$
$$= \int d\mathbf{x}' d\mathbf{x}'' \, G_{ik}^{\text{E}}(\mathbf{x}, \mathbf{x}') G_{j\ell}^{\text{M}*}(\mathbf{x}, \mathbf{x}'') \left\langle J_k(\mathbf{x}') J_\ell(\mathbf{x}'') \right\rangle$$

Inserting (2),

$$= \int d\mathbf{x}' G_{ik}^{\text{E}}(\mathbf{x}, \mathbf{x}') G_{jk}^{\text{M}*}(\mathbf{x}, \mathbf{x}') \Theta\big[\omega, T(\mathbf{x}')\big] \sigma(\omega, \mathbf{x}') \quad (7)$$

where $T(\mathbf{x})$ is the local temperature and $\Theta\big[\omega, T\big] = \frac{\hbar\omega}{2\pi} \coth \hbar\omega / 2kT$ is the statistical factor in equation (2). (Summation over repeated tensor indices is implied here and throughout.)

The obvious advantage of an equation like (7) is that it reduces a problem in quantum statistical mechanics (determination of the electromagnetic field fluctuations at $\mathbf{x}$) to a problem in classical electromagnetic scattering (computation of the DGFs $G^{\text{E,M}}$). The difficulty of this approach lies in the great *number* of scattering problems that must be solved. Indeed, equation (7) says that, to compute the Poynting flux at a single point $\mathbf{x}$, we need the DGFs connecting $\mathbf{x}$ to *all points* $\mathbf{x}'$ at which the conductivity is nonvanishing; for a typical problem involving two dissipative bodies in vacuum, this amounts to a solving a separate scattering problem for each point in the volume of each body. Moreover, even

after completing all of these calculations we have still only computed the Poynting flux at a single point $\mathbf{x}$; in general we will want to integrate this flux over a surface to get the total power transfer at a given frequency, and subsequently to integrate over all frequencies to get the total power transfer.

Thus the fluctuation-dissipation concept, in the form of equations (2) or (7), performs the great *conceptual* service of reducing predictions of noise phenomena to problems of classical electromagnetic scattering, but leaves in its wake the *practical* problem of how to solve the formidable number of scattering problems that result. This difficulty has been addressed in a variety of ways, some of which we will review in the following sections.

III. NEAR-FIELD HEAT RADIATION: FLUCTUATION-INDUCED ENERGY TRANSFER IN NANOSCOPIC SYSTEMS

Fluctuating currents in finite-temperature bodies give rise to radiated fields which carry away energy. If there are other bodies (or an embedding environment) present at the same temperature, then any energy lost by one body to radiation is replenished by an equal energy absorbed from the radiation of other bodies. However, between objects at *different* temperatures there is a net transfer of power, whose rate we can calculate in terms of the temperatures and electromagnetic properties of the bodies.

Historically, the first step in this direction was the *Stefan-Boltzmann law*, a triumph of 19th-century physics which held that the power radiated per unit surface area of a temperature-T body was simply $\eta \sigma_{\text{SB}} T^4$, where σ_{SB} is a universal constant and η, the *emissivity*, is a dimensionless number between 0 and 1 characterizing the electrical properties of the body (specifically, its propensity to emit radiation relative to that of a perfect emitter or *black body*). The Stefan-Boltzmann prediction is based on an approximation that simplifies the electromagnetic analysis: it considers only *propagating* electromagnetic waves, neglecting the *evanescent* portions of the $\mathbf{E}$ and $\mathbf{H}$ fields that exist in the vicinity of object surfaces. This is a good approximation when computing the power transfer between a single body and its environment, or between two inequal-temperature bodies separated by large distances.

However, when inequal-temperature bodies are separated by short distances, evanescent fields can contribute significantly to the Poynting flux and the rate of power transfer may deviate significantly from the Stefan-Boltzmann prediction. The length scale below which distances are to be considered "short" is the *thermal wavelength,*

$$\lambda_T = \frac{\hbar c}{kT} \approx 7.6\,\mu\text{m} \cdot \left(\frac{300\text{ K}}{T}\right),$$

and thus, in practice, observing deviations from the Stefan-Boltzmann law requires measuring the heat flux between two bodies maintained at inequal temperatures and at a surface–surface separation of a few microns. This formidable experimental challenge has recently been met by several groups [2], [26], and this progress has spurred the development of new theoretical techniques for predicting the heat flux between

closely-spaced bodies with realistic material properties and various shapes, which we now describe.

A. Radiative Heat Transfer as a Scattering Problem

Consider two homogeneous bodies $\mathcal{B}_{1,2}$ separated by a short distance and maintained at separate internal thermal equilibria at temperatures $T_{1,2}$. (We will consider the bodies to exist in vacuum; the case of a finite-temperature embedding environment is a straightforward generalization.) The rate at which energy is absorbed or lost by body 1 is given as a surface integral of the mean Poynting flux,

$$P_1(\omega) = \frac{1}{2} \int_{\mathcal{S}_1} \left\langle \mathbf{E}(\omega, \mathbf{x}) \times \mathbf{H}^*(\omega, \mathbf{x}) \right\rangle \cdot d\mathbf{S}, \qquad (8)$$

where $\mathcal{S}_1$ is the surface of body 1 (or, equivalently, a fictitious bounding surface containing body 1 and no other bodies) and $d\mathbf{S}$ is the inward-pointing surface normal. Applying equation (7) reduces the quantity in brackets to integrals over the volumes of the bodies (again suppressing ω arguments to G):

$$P_1(\omega) \qquad\qquad\qquad\qquad\qquad\qquad\qquad (9)$$
$$= \frac{\varepsilon_{ijk}}{2} \int_{\mathcal{S}_1} \left\{ \sigma_1(\omega) \Theta[\omega, T_1] \int_{\mathcal{B}_1} G_{i\ell}^{\text{E}}(\mathbf{x}, \mathbf{x}') G_{j\ell}^{\text{M}*}(\mathbf{x}, \mathbf{x}')\, d\mathbf{x}' \right.$$
$$\left. + \sigma_2(\omega) \Theta[\omega, T_2] \int_{\mathcal{B}_2} G_{i\ell}^{\text{E}}(\mathbf{x}, \mathbf{x}') G_{j\ell}^{\text{M}*}(\mathbf{x}, \mathbf{x}')\, d\mathbf{x}' \right\} dS_k.$$

where $\sigma_{1,2}$ are the conductivities of the bodies. [Here we have used the Levi-Civita symbol ε_{ijk} to write the components of the cross product as $(\mathbf{A} \times \mathbf{B})_k = \varepsilon_{ijk} A_i B_j$.] Note that equation (9) includes integrations over the volumes of *both* bodies, since there are fluctuating sources present in both bodies. Intuitively one might expect that reciprocity arguments could be exploited to relate the two terms to one another and hence streamline the calculation to involve integration over just one body; this intuition is indeed born out in practice, as discussed below [15].

Equation (9) reduces the calculation of the net energy transfer to or from a body to the classical electromagnetic scattering problem of computing the DGFs for a geometry consisting of our two material bodies $\mathcal{B}_{1,2}$. The difficulty, as anticipated above, is that we must solve a great number of scattering problems; in principle, for each surface point $\mathbf{x}$ and each volume point $\mathbf{x}'$ in the combined surface–volume integrals in (9) we must solve a separate scattering problem (computing the fields at $\mathbf{x}$ due to individual point sources at $\mathbf{x}'$). This challenge is in fact so formidable that computations for geometries even as simple as two spheres have only become available in the past few years, using techniques which we now review.

B. Semi-Analytical Approaches to Radiative Transfer

A first strategy for evaluating (9) is to consider certain highly symmetric geometries for which a convenient choice of coordinates allows the DGFs to be evaluated analytically. For example, the earliest near-field heat-transfer calculations [12], [13] took the two objects to be semi-infinite planar slabs, in which case the DGFs are analytically calculable. More

recently, several groups have extended this approach to other highly symmetric geometries in which special-function expansions of the DGFs are available [14], [27]–[32]. A particularly convenient tool here is the "matrix" approach to electromagnetic scattering, a technique first discussed in these PROCEEDINGS in 1965 [33]. To solve scattering problems in this approach, one begins by writing down two sets of functions, $\{\mathbf{E}_n^{\text{in}}(\mathbf{x})\}$ and $\{\mathbf{E}_n^{\text{out}}(\mathbf{x})\}$; these are solutions of Maxwell's equations, in an appropriate coordinate system, which respectively describe electromagnetic waves propagating *inward* from infinity to our scattering geometry and *outward* from the scatterer into open space. (For example, in spherical geometries the $\{\mathbf{E}_n\}$ will be products of vector spherical harmonics and spherical Bessel functions [18].) The disturbance in the electromagnetic field due to a scattering object is then entirely encapsulated in the object's *T-matrix*, denoted $\mathbb{T}$, whose m, n element gives the amplitude of the mth outgoing wave for a scatterer illuminated by the nth incoming wave. In other words,

if the incident field is $\mathbf{E}^{\text{inc}}(\mathbf{x}) = \mathbf{E}_n^{\text{in}}(\mathbf{x})$

then the scattered field is $\mathbf{E}^{\text{scat}}(\mathbf{x}) = \sum_m \mathbb{T}_{mn} \mathbf{E}_m^{\text{out}}(\mathbf{x}).$

Because the T-matrix for a body encodes all information needed to understand its scattering properties, it is often possible to express the solution to a radiative-transfer problem in terms of simple matrix operations on the T-matrices of the objects involved. As an illustration of the sort of concise expression that can result from this procedure, the methods of Ref. [27] lead to a simple trace formula for the spectral density of heat radiation from a single sphere at temperature T [34]:

$$H(\omega, T) = -2\Theta'[\omega, T] \sum_n \left\{ \text{Re } \mathbb{T}_{nn}(\omega) + |\mathbb{T}_{nn}(\omega)|^2 \right\} \tag{10}$$

where $\mathbb{T}$ is the T-matrix of the sphere, the sum runs over its diagonal elements, and Θ' is just Θ minus the contribution of the zero-point energy term.

The obvious advantage of an equation like (10) is that it is simple enough to be implemented in a few lines of MATHEMATICA or MATLAB for objects whose T-matrix is known analytically. The difficulty is that there are not many such objects; indeed, the only lossy scatterers for which the T-matrix may be obtained in closed form are spheres, infinite-length cylinders, and semi-infinite slabs. (Idealizing the materials as lossless metals extends the list of shapes for which the T-matrix is known analytically [35], but this is not useful for radiative-transfer problems because lossless materials neither absorb nor radiate energy.) To make predictions for shapes outside this narrow catalog we must turn instead to numerical methods.

C. Numerical Approaches to Radiative Transfer

One approach to numerical heat-transfer modeling is to combine matrix-trace formulas in the spirit of equation (10) with a numerical technique for computing the T-matrices
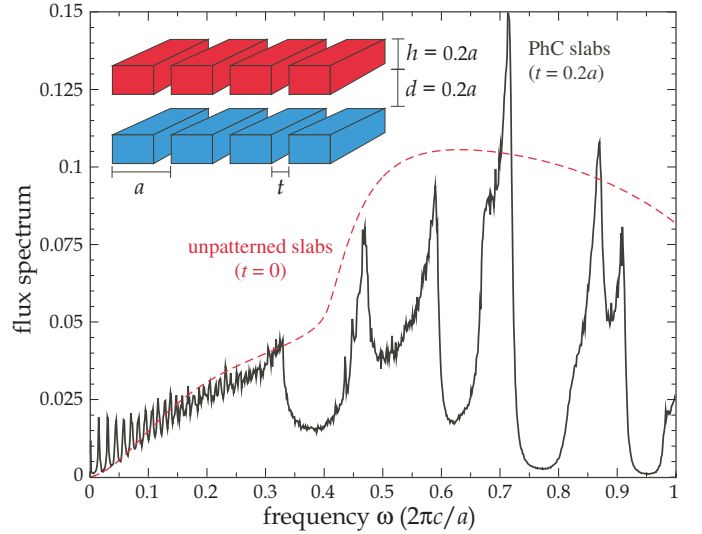

Fig. 3.   Near-field radiative heat transfer between patterned and unpatterned SiC slabs [15]. The solid black curve plots the spectral density of power flux between SiC photonic crystals (inset) maintained at inequal temperatures and surface–surface separation d. The dashed red curve plots the power flux between unpatterned SiC slabs. (In both cases, the power flux is normalized by the power flux that would obtain between the same structures at infinite separations $d \to \infty$.)

of irregularly-shaped objects. This technique was pursued in Ref. [16], which investigated heat transfer from hot tips of various shapes to a cool planar substrate at micron-scale distances. In this work, a boundary-element scattering code was used to compute numerical T-matrices for finite cylinders and finite-length cones; a surprising conclusion was that conical tips, despite tapering to a point, nonetheless exhibit *less* spatial concentration (i.e. a larger and more diffuse spot size) of heat transferred to the substrate as compared to cylindrical tips.

An alternative numerical approach to heat-transfer calculations is to bypass the T-matrix approach in favor of a more direct assault on equation (9) [15], [36]; here a "brute-force" approach can deliver great generality with minimal programming time, at the expense of much computer time. Physically, the situation described by equation (9) is that we have randomly fluctuating currents distributed throughout the interior of our material bodies, and we wish to compute the fields to which these currents give rise. A particularly convenient way to do this computation is to run a time-domain simulation, in which we calculate the fields due to a random time-varying current distribution whose correlation function in the frequency domain satifies equation (2); by repeating this calculation for many randomly-generated current distributions and averaging the results, we obtain approximate ensemble averages of the time-domain $\mathbf{E}$ and $\mathbf{H}$ fields, which we may then Fourier-analyze to obtain frequency spectra. This approach is rendered computationally feasible by exploiting several properties of equation (2) and of Maxwell's equations. First, *absence of spatial correlation*: the δ function in (2) ensures that currents at different locations in space (in particular, currents in different bodies) are uncorrelated and may thus be chosen to have independent random phases. Second, *linearity*: although equation (2) calls for stochastic currents with non-flat

spectral density shaped by the factor $\Theta[\omega, T]$—what engineers might think of as "colored noise"—the linearity of Maxwell's equations ensures that we can instead compute the fields due to *white-noise* currents, which are significantly easier to generate in the time domain, and only later multiply the resulting frequency spectrum by the appropriate shaping factor. Finally, *reciprocity*: the flux absorbed by body $\mathcal{B}_2$ due to radiating sources in $\mathcal{B}_1$ is equal to the flux absorbed by $\mathcal{B}_1$ due to sources in $\mathcal{B}_2$. This observation allows us to place our stochastic sources only in $\mathcal{B}_1$ and compute the resulting flux only into $\mathcal{B}_2$.

Combining these arguments leads to a simple expression for the spectral density of the net heat flux between bodies [15]:

$$H(\omega, T_1, T_2) = \Phi(\omega)\Big\{ \Theta\big[\omega, T_1\big] - \Theta\big[\omega, T_2\big] \Big\}$$

where Φ is the flux into one of the objects due to random (white-noise) current sources in the other object. In practice, Φ is computed using a finite-difference time-domain technique, with random current sources placed at grid points throughout the volume of the bodies and the results averaged over many (~ 60) simulations.

Fig. 3 illustrates the type of result that may be obtained using this method [15]. The solid curve in the figure plots the spectral density of power flux between two one-dimensional photonic crystals of SiC separated by a short distance d (inset). The dashed curve plots the power flux between *unpatterned* SiC slabs. (In both cases, the power flux is normalized by the flux between the same structures at infinite separation $d \to \infty$.) The patterning of the slabs drastically modifies the flux spectrum as compared to the unpatterned case.

IV. CASIMIR FORCES: FLUCTUATION-INDUCED MOMENTUM TRANSFER IN NANOSCOPIC SYSTEMS

In the previous section, we considered applications of fluctuation-dissipation ideas to situations out of thermal equilibrium, and we noted the fierce computational challenges that arise from the need to solve separate scattering problems for each point in the volume integration in (7). At thermal equilibrium, a major simplification occurs which significantly reduces computational requirements. The situation is most clearly displayed by considering the mean product of **E**-field components, which reads, in close analogy to (7),

$$\big\langle E_i(\mathbf{x}) E_j^*(\mathbf{x}') \big\rangle \tag{11}$$
$$= \int d\mathbf{y}\, G_{ik}^{\mathrm{E}}(\mathbf{x}, \mathbf{y}) G_{jk}^{\mathrm{E}*}(\mathbf{x}', \mathbf{y}) \Theta\big[\omega, T(\mathbf{y})\big] \sigma(\omega, \mathbf{y})$$

The key point is that, at thermal equilibrium, $T(\mathbf{y}) \equiv T$ is spatially constant, whereupon the statistical factor may be pulled out of the integral to yield

$$= \Theta[\omega, T] \int d\mathbf{y}\, G_{ik}^{\mathrm{E}}(\mathbf{x}, \mathbf{y}) G_{jk}^{\mathrm{E}*}(\mathbf{x}', \mathbf{y}) \sigma(\omega, \mathbf{y})$$
$$= \frac{1}{\omega} \Theta[\omega, T] \operatorname{Im} G_{ij}^{\mathrm{E}}(\mathbf{x}, \mathbf{x}'). \tag{12}$$

(In going to the last line here we used a standard identity in electromagnetic theory which follows directly from Maxwell's equations [37].) Thus, evaluating a mean product of field components at thermal equilibrium requires the solution of only a *single* scattering problem, in contrast to the formally infinite number of scattering problems required for out-of-equilibrium situations.

Of course, the heat-transfer calculations of the previous section are not very interesting at thermal equilibrium, in which by definition there can be no net transfer of energy between bodies. However, a different sort of fluctuation-induced phenomenon—the *Casimir effect*—gives rise to non-trivial interactions among bodies even at the same temperature (and even at zero temperature), and constitutes a second major branch of the study of electromagnetic fluctuations.

A. The Casimir Effect

In 1948 [38], Casimir and Polder generalized the van der Waals (or "London dispersion") force between fluctuating dipoles of molecules and other small particles, which depends on the distance r between the particles like $1/r^7$, to a "retarded" force that varies like $1/r^8$ at large distances (typically tens of nanometers) where the finite speed of light must be taken into account. Later that year [4], Casimir considered the region between two parallel mirrors as a type of electromagnetic cavity, characterized by a set of cavity-mode frequencies $\{\omega(d)\}$ depending on the mirror separation distance d. By summing the zero-point energies [equation (3a)] of all modes and differentiating with respect to d, Casimir predicted an attractive pressure between the plates of magnitude

$$\frac{F}{A} = \frac{\pi^2 \hbar c}{240 d^4} \approx \frac{10^{-8}\ \mathrm{atm}}{(d\ \mathrm{in}\ \mu\mathrm{m})^4}, \tag{13}$$

negligible at macroscopic distances but significant for surface–surface separations below a few hundred nanometers.

The Casimir effect was subsequently reinterpreted [39], [40] as an interaction among fluctuating charges and currents in material bodies, a perspective which allows the use of fluctuation-dissipation formulas like (12) to predict Casimir forces in situations where the cavity-mode picture would be unwieldy. In fact, the Casimir effect has been interpreted in a bewildering variety of ways; in addition to the zero-point-energy picture of Ref. [4] and the source-fluctuation picture of Ref. [39], there are path-integral formulations [23], world-line methods [41], and ray-optics approaches [42], to name but a few. Each of these perspectives emphasizes different aspects of the underlying physics, although of course all physical interpretations lead ultimately to mathematically equivalent final results [24]. However, despite the plethora of theoretical perspectives, and even with the simplifications afforded by thermal equilibrium, the calculations remained so challenging that force predictions for all but the simplest geometries were practically out of reach, and—with experimental progress hampered by the difficulty of measuring nanonewton forces between bodies at sub-micron distances—for many decades there was little demand for computational Casimir methods that could handle general geometries and materials.

This situation began to change about 15 years ago with the advent of precision Casimir metrology [43], and since that

time the Casimir effect has been experimentally observed in an increasingly wide variety of geometric and material configurations (for recent reviews of experimental Casimir physics, see [17], [44]). This experimental progress has spurred the development of theoretical techniques capable of predicting Casimir forces and torques in complex, asymmetric geometries with realistic materials, which we now review.

B. The Casimir Effect as a Scattering Problem

As in Section III-A, we consider two bodies $\mathcal{B}_{1,2}$ in vacuum. In equation (8) we integrated the average Poynting flux over a surface surrounding a body to obtain the rate of energy transfer to that body. To compute the rate of *momentum* transfer to the body—that is, the force on the body—we proceed analogously, but now instead of the Poynting flux we integrate the average Maxwell stress tensor:

$$\boldsymbol{\mathcal{F}}(\omega) = \int_{\mathcal{S}} \Big\langle \mathbf{T}(\omega, \mathbf{x}) \Big\rangle \cdot d\mathbf{S}, \qquad (14)$$

where the components of $\mathbf{T}$ are given in terms of the components of $\mathbf{E}$ and $\mathbf{H}$ as

$$T_{ij} = \epsilon_0 E_i E_j + \mu_0 H_i H_j - \frac{\delta_{ij}}{2}\Big[\epsilon_0 E_k E_k + \mu_0 H_k H_k\Big].$$

Inserting (12) and its magnetic analogue into (14) now yields an expression analogous to (9)—but simplified by the absence of volume integrals—which at temperature $T = 0$ takes the form, for the i component of the force,

$$\mathcal{F}_i(\omega) = \frac{\hbar\omega}{\pi}\mathrm{Im} \int_{\mathcal{S}} \Big\{ \epsilon_0 \, \mathcal{G}_{ij}^{\mathrm{E}}(\omega, \mathbf{x}, \mathbf{x}) + \mu_0 \, \mathcal{G}_{ij}^{\mathrm{H}}(\omega, \mathbf{x}, \mathbf{x}) \quad (15)$$
$$- \frac{\delta_{ij}}{2}\Big[\epsilon_0 \, \mathcal{G}_{kk}^{\mathrm{E}}(\omega, \mathbf{x}, \mathbf{x}) + \mu_0 \, \mathcal{G}_{kk}^{\mathrm{H}}(\omega, \mathbf{x}, \mathbf{x})\Big] \Big\} dS_j.$$

Here $\mathcal{G}(\mathbf{x}, \mathbf{x}')$, the *scattering part* of a DGF G, is the contribution to G which remains finite as $\mathbf{x}' \to \mathbf{x}$; this is just the field at $\mathbf{x}$ due to currents *induced* by a point source at $\mathbf{x}'$, but neglecting the *direct* contribution of that point source. [In (15), $\mathcal{G}^{\mathrm{H}}$ is the scattering part of the DGF that relates magnetic fields to magnetic currents.]

Equation (15), like equation (9), reduces our problem to that of determining the DGFs for our material configuration, and in principle we could now proceed to evaluate the surface integral in (15) with the integrand computed by standard scattering techniques. For Casimir calculations, however, the situation is complicated by an important subtlety, which we now discuss.

C. Transition to the Imaginary Frequency Axis

In contrast to the heat-transfer problems discussed in the previous section, for Casimir problems we will not typically be interested in the contributions of individual frequencies but will instead seek only the *total* Casimir force on a body, obtained by integrating (15) over all frequencies:

$$F_i = \int_0^{\infty} \mathcal{F}_i(\omega) \, d\omega. \qquad (16)$$

But naïve attempts to evaluate equation (16) numerically are doomed to failure by the existence of rapid oscillations in the integrand, as pictured in Fig. 4**a** for the particular case of
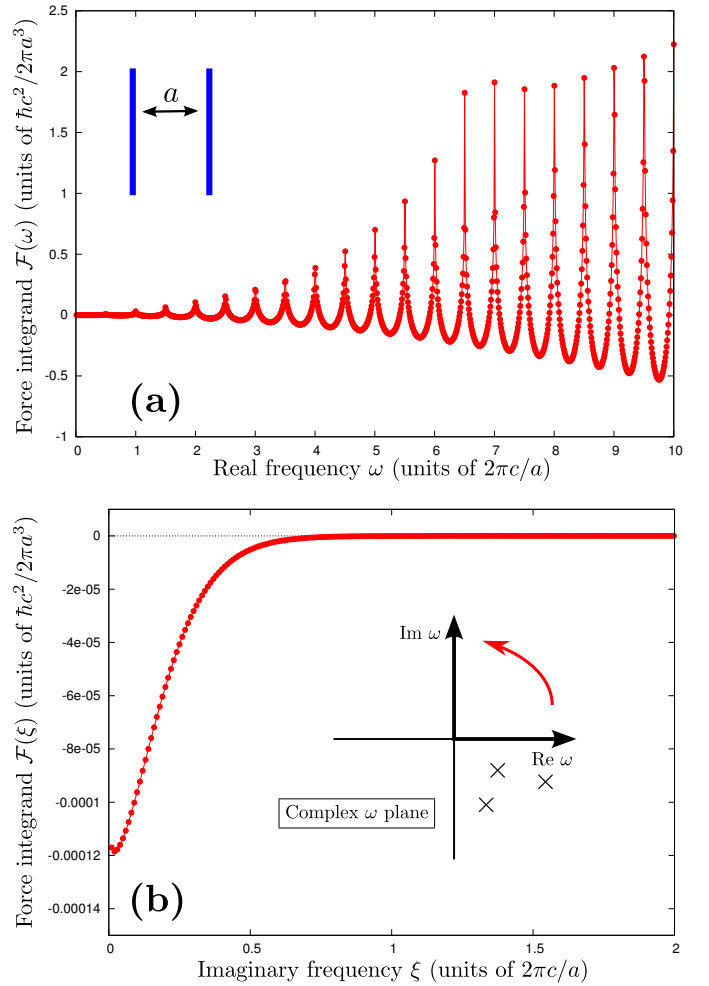

Fig. 4. Transition to the imaginary frequency axis. **(a)** As a function of real frequency ω, the Casimir force integrand $\mathcal{F}(\omega)$ of equation (15)—shown here for the case of parallel metallic plates separated by a distance a (inset)—exhibits severe oscillations which effectively prohibit evaluation of the integral (16) by numerical quadrature. (For the particular case of parallel plates, the expression for the Casimir force integrand is known as the *Lifshitz formula* [40].) These oscillations are associated with cavity resonances, which show up mathematically as poles in the lower half of the complex frequency plane (inset); the real part of the pole corresponds to the resonance frequency, while the imaginary part corresponds to the width (or the inverse lifetime) of the resonance. **(b)** Rotating to the *imaginary* frequency axis (inset) moves the contour of integration away from the cavity-resonance poles, resulting in a smooth integrand that succumbs readily to numerical quadrature.

the Casimir force between parallel metallic plates in vacuum. The origin of these oscillations is not hard to identify: they are related to the existence of electromagnetic *resonances* in our scattering geometry, which correspond mathematically to poles of the integrand in the lower half of the complex ω plane. (The oscillatory nature of the force spectrum was emphasized in Ref. [45], and the implications for numerical computations were discussed in Ref. [46].)

But this diagnosis of the problem suggests a cure: thinking of (16) as a contour integral in the complex frequency plane, we simply rotate the contour of integration 90 degrees and integrate over the *imaginary* frequency axis (Fig. 4**b**). This

procedure, known in physics as a *Wick rotation* [47], yields

$$F_i = \int_0^\infty \mathcal{F}_i(\xi)\, d\xi \qquad (17)$$

where $\omega = i\xi$ and $\mathcal{F}$ now involves the DGFs evaluated at imaginary frequencies:

$$\mathcal{F}_i(\xi) = \frac{\hbar\xi}{\pi} \int_{\mathcal{S}} \left\{ \epsilon_0\, \mathcal{G}_{ij}^{\mathrm{E}}(\xi, \mathbf{x}, \mathbf{x}) + \mu_0\, \mathcal{G}_{ij}^{\mathrm{H}}(\xi, \mathbf{x}, \mathbf{x}) \right. \qquad (18)$$
$$\left. - \frac{\delta_{ij}}{2} \left[\epsilon_0\, \mathcal{G}_{kk}^{\mathrm{E}}(\xi, \mathbf{x}, \mathbf{x}) + \mu_0\, \mathcal{G}_{kk}^{\mathrm{H}}(\xi, \mathbf{x}, \mathbf{x}) \right] \right\} dS_j.$$

The Wick rotation is possible here because the DGFs are analytic functions in the upper half of the complex ω plane. This is a well-known consequence of causality: the fields arise after the current fluctuations that generate them [48]. Another consequence of causality is that, for passive materials, the permittivity and permeability functions on the imaginary frequency axis $\{\epsilon(i\xi), \mu(i\xi)\}$ are guaranteed to be real-valued and positive [49].

Physically, the transition to the imaginary frequency axis corresponds to replacing the oscillatory time dependence $\sim e^{-i\omega t}$ of all fields and currents with an exponentially *growing* time dependence $\sim e^{+\xi t}$; for frequency-domain computational electromagnetism, this has the effect of replacing the spatially oscillatory Helmholtz kernel ($\frac{e^{i\omega r/c}}{4\pi r}$) with an exponentially *decaying* kernel ($\frac{e^{-\xi r/c}}{4\pi r}$). As illustrated in Fig. 4**b**, the imaginary-frequency Casimir force integrand $\mathcal{F}(\xi)$ is a well-behaved smooth function that succumbs readily to numerical quadrature.

Equations (17) and (18) are valid at zero temperature. At finite temperatures $T > 0$, we must include a factor $\Theta[\xi, T] \sim \coth i\hbar\xi/2kT$ under the integral sign; in this case, it is well-known in physics [40] that the integral (17) over the imaginary frequency axis may be evaluated using the method of residues to obtain

$$F_i = \frac{2\pi kT}{\hbar} \sum_{n=0}^{\infty}{}' \mathcal{F}_i(\xi_n) \qquad (19)$$

where $\xi_n = 2n\pi kT/\hbar$, the *Matsubara frequencies*, are just the poles of the $\coth$ factor on the imaginary frequency axis. [The primed sum in (19) indicates that the $n = 0$ term enters with weight 1/2.] Computationally, the upshot of equation (19) is that finite-temperature Casimir forces are computed with no more conceptual difficulty than zero-temperature forces, with the integral in (17) simply replaced by the sum in (19), although the need to evaluate equation (18) in the limit of zero frequency ($\xi = 0^+$) poses challenges for some methods of computational electromagnetism [50], [51]. The temperature dependence of Casimir interactions is a topic of recent theoretical [52] and experimental [53] interest.

D. Semi-Analytical Approaches to Casimir Computations

Like the first studies of near-field radiative transfer, the first generation of theoretical Casimir techniques focused on highly symmetric geometries for which analytical scattering solutions are available [22], [23], [28], [54]–[58]. As an example of the type of concise expression that may be obtained via these methods, the zero-temperature Casimir force between two compact bodies with center–center separation vector $\mathbf{R}$ may be expressed in the form [9]

$$F_i = \frac{\hbar}{2\pi} \int_0^\infty \mathrm{Tr}\, \left[\mathbb{M}^{-1}(\xi) \cdot \frac{\partial \mathbb{M}(\xi)}{\partial \mathbf{R}_i} \right] d\xi \qquad (20)$$

where the matrix $\mathbb{M}$ has the block structure

$$\mathbb{M} = \left(\begin{array}{cc} \mathbb{T}_1^{-1} & \mathbb{U}(\mathbf{R}) \\ \mathbb{U}^\dagger(\mathbf{R}) & \mathbb{T}_2^{-1} \end{array} \right);$$

here $\mathbb{T}_n$ is the T-matrix for body n and $\mathbb{U}(\mathbf{R})$ is a *translation matrix*, which relates spherical Helmholtz solutions about different origins and for which closed-form analytic expressions are available [59]. [The partial derivative in (20) is taken with respect to a rigid displacement of one body in the ith cartesian direction.]

Like equation (10), the formula (20) is simple enough that it can be implemented in just a few lines of MATHEMATICA or MATLAB code for geometries in which the $T-$matrix is known analytically. Again, however, such geometries are rare, and for more complicated geometric configurations we must turn to numerical methods.

E. Numerical Approaches to Casimir Computations

The most direct way to apply numerical techniques to Casimir computations is simply to evaluate the surface integral in (18) by numerical cubature, with the $\mathcal{G}$ tensors at each integrand point $\mathbf{x}$ evaluated by solving a numerical scattering problem in which we place a point source at $\mathbf{x}$ and compute the scattered fields back at the same point $\mathbf{x}$. In principle, this scattering problem may be solved by any of the myriad available techniques for numerical solution of scattering problems (although the need for imaginary-frequency calculations poses something of a limitation in practice). To date, computational Casimir methods based on numerical evaluation of (18) have been implemented using a variety of standard techniques in computational electromagnetism: the finite-difference frequency-domain method [46], [60], the finite-difference time-domain method [with some transformations to convert the integral over frequencies in (18) into an integral over the time-domain response of a current pulse] [61]–[63], and the boundary-element method [64], [65].

Compared to the special-function approaches discussed in Section IV-D, any one of these numerical methods offers the significant practical advantage of handling arbitrarily complex geometries with little more difficulty than simple geometries. Among the various numerical methods, the finite-difference methods have the advantage of greater generality—in the sense that they can readily handle arbitrarily complex material configurations, including anisotropic and continuously-varying dielectrics—while the boundary-element methods have the advantage of greater computational efficiency for the piecewise-homogeneous material configurations typically encountered in practice.

As an illustration of the type of problem that is facilitated by numerical Casimir methods, Figure 5 plots the force between
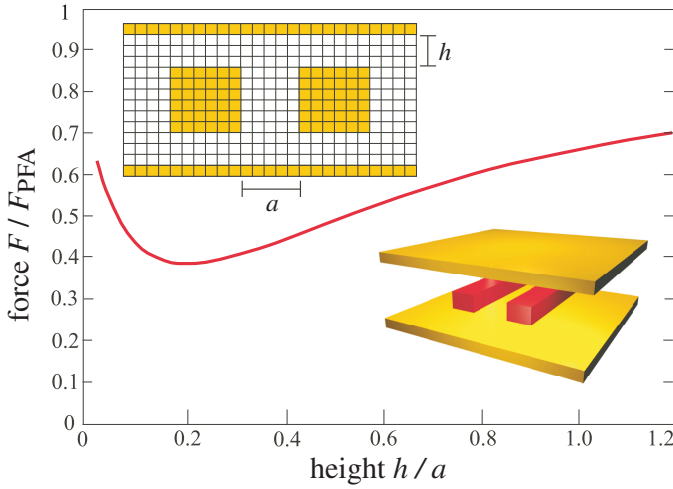
Fig. 5. Casimir force between elongated pistons confined between parallel plates [46]. The lower inset depicts the geometry, while the upper inset shows the finite-difference grid used to model the cross-section of this z-invariant structure. The force between the pistons exhibits a suprising *non-monotonic* dependence on the separation distance h between the pistons and the plates. [The quantity plotted is the actual force divided by the proximity-force approximation (PFA) to the force, a convenient h-independent normalization.]
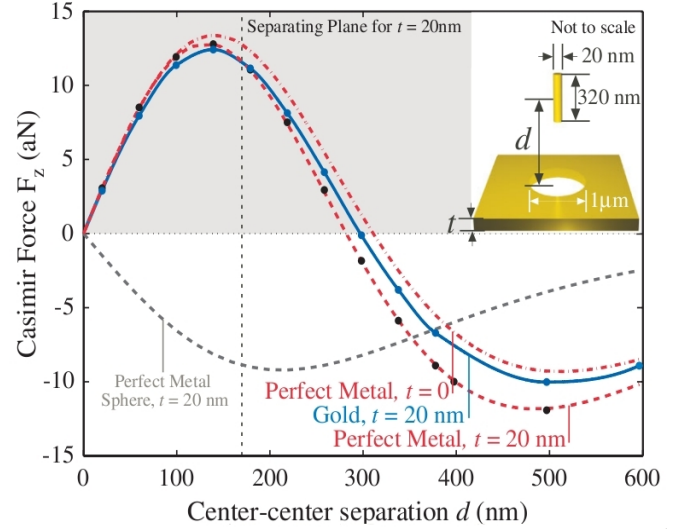

Fig. 6. Repulsive Casimir force between metallic objects in vacuum. Plotted is the z-directed force on an elongated nanoparticle above a circular aperture in a metallic plate (inset), as a function of the separation distance d between the center of the nanoparticle and the center of the plate. The dashed red curves are for the case of perfectly conducting materials (for two different plate thicknesses), while the solid blue curve is for the case of finite-conductivity gold. The shaded region of the force curve indicates the repulsive regime, in which the nanoparticle is repelled from the plate. (The dashed vertical line denotes the *separating plane*, i.e. the value of d beyond which the nanoparticle is entirely above the plate.) For comparison, the dashed grey curve indicates the force on a perfectly-conducting *spherical* nanoparticle; in this case the force is attractive at all separations. (Figure reproduced from Ref. [11].)

elongated square pistons confined between parallel plates (all bodies are perfect conductors), as computed using a finite-difference technique [46]. The lower inset in the figure depicts the geometry, while the upper inset shows the finite-difference grid used to model the cross-section of this z-invariant structure. The force between the pistons exhibits a suprising *non-monotonic* dependence on the separation distance h between the pistons and the plates.

F. Fluctuating-Surface-Current Approach to Casimir Computations

The finite-difference and boundary-element methods described above have the advantage of great generality, in that they treat bodies of arbitrarily complex shapes with no more difficulty than simple symmetric bodies. However, the need for numerical evaluation of the surface integral in (18) adds a layer of conceptual and computational complexity that is absent from the concise expression (20).

An alternative is the recently developed *fluctuating-surface-current* approach [10], [66]–[68]. In the FSC technique, we begin with a boundary-element-method (BEM) approach to evaluating the DGFs in (18). Instead of proceeding numerically, however, we exploit the structure of the BEM technique to obtain compact analytical expressions for the DGFs in fully-factorized form, involving products of factors depending separately on the source and evaluation points. Inserting these expressions into (18) then turns out to allow the surface integral to be evaluated *analytically*, in closed form, leaving behind only straightforward matrix manipulations [67], [68]. The final FSC formula for the Casimir force,

$$F_i = \frac{\hbar}{2\pi} \int_0^\infty \text{Tr} \left[\mathbf{M}^{-1}(\xi) \cdot \frac{\partial \mathbf{M}(\xi)}{\partial \mathbf{R}_i} \right] d\xi, \qquad (21)$$

bears a remarkable similarity to (20), but now with a different matrix $\mathbf{M}$ entering into the matrix manipulations; whereas

$\mathbb{M}$ in (20) describes the interactions between incoming and outgoing waves in a multipole expansion of the electromagnetic field, $\mathbf{M}$ in (21) describes the interactions among *surface currents* flowing on the surfaces of the interacting objects in a Casimir geometry. [$\mathbf{M}(\xi)$ in (21) is just the usual impedance matrix that enters into the PMCHW formulation of the boundary-element method [69], but now evaluated at imaginary frequencies.]

As one example of the type of calculation that is facilitated by FSC Casimir techniques, Ref. [11] investigated the Casimir force on an elongated nanoparticle above a circular aperture in a metallic plate and identified a region of the force curve in which the force on the particle is *repulsive* (Fig. 6). This geometry is notable as the only known configuration exhibiting repulsive Casimir forces between non-interleaved metallic objects in vacuum. (On the other hand, repulsive forces between dielectric objects immersed in a dielectric liquid have long been known to exist and were observed experimentally in 2009 [70]; in addition, numerical Casimir tools have been used to demonstrate theoretically the possibility of achieving stable suspension of objects in fluids [71], and further work in this area may have applications in microfluidics.)

V. Summary and Outlook

Despite spending most of its history confined to the realm of pure physics, the theory and experimental characterization of fluctuation-induced electromagnetic phenomena is at last poised to take on a new role as a growth area in electrical

engineering. The growing ease and ubiquity of nanotechnology are making near-field radiative transport and Casimir forces increasingly relevant to the technologies of today and tomorrow, with a corresponding imminent need for engineers to account for these phenomena in their designs. In this connection it is convenient that a host of powerful computational methods, inspired by techniques of classical computational electromagnetism but extending these methods in several ways, have been developed over the past several years to model various fluctuation phenomena. We hope to have convinced the reader that the sudden conjunction of new theoretical techniques, increasing experimental relevance, and the paucity of known results have created burgeoning opportunities for computational science—indeed, in fields where two spheres represent a novel geometry, the untapped frontiers of design are vast and inviting.

What lies in store for the future of this field? The work reviewed in this article has answered many questions, only to pose many more to be addressed in the coming years. Here we give a brief flavor of some challenges that lie on the horizon.

General-basis trace formulas for heat transfer. Unlike Casimir forces, the theory of near-field radiation does not yet benefit from a compact trace formula that applies to an arbitrary localized basis. Existing approaches either require the intermediary of a spectral incoming/outgoing wave basis (such as cylindrical or spherical waves) that may be ill-suited for irregular geometries, or large-scale computations involving costly integral evaluations. Is a synthesis (in the spirit of the FSC approach of Section IV-F) possible or practical, and what form does it take?

Fast solvers. To date, practical applications of integral-equation Casimir techniques have evaluated the matrix operations in equation (21) (matrix inverse, matrix multiplication, and matrix trace) using methods of dense-direct linear algebra. These methods are appropriate for matrices of moderate dimension ($D \sim 10^4$ or less), but for larger problems the $O(D^2)$ memory scaling and $O(D^3)$ CPU-time scaling of dense-direct linear algebra renders calculations intractable. A similar bottleneck was encountered many years ago in the computational electromagnetism community, where it was remedied by the advent of *fast solvers*—techniques such as the fast multipole [72] and precorrected-FFT [73] methods that employ matrix-sparsification techniques to reduce the asymptotic complexity scaling of matrix operations to more manageable levels; $O(D^{3/2} \log D)$ [74] or $O(D \log D)$ [75], [76] are typical. Although such methods could, in principle, be applied to stress-tensor Casimir computations [46], [64], can they be made practical? Can they be applied to the FSC trace-formula approach, and with what performance implications?

New experimental geometries. Until recently, theoretical techniques in fluctuation-induced phenomena lagged behind the forefront of experimental progress (indeed, as we have seen, it is only in the past few years that complete theoretical solutions for the simple sphere–plate geometry commonly seen in experiments have become available). This situation has recently begun to change; with a host of new computational methods for near-field radiative transfer and Casimir phenomena becoming available in the past five years, we are entering an era in which theoretical predictions can be used

to guide the design of future experiments—and, ultimately, future technologies. Such a reversal is not without precedent in the history of electrical engineering. Indeed, whereas the first computational algorithms for modeling antennas and transistor circuits were validated by checking that they correctly reproduced the behavior of existing laboratory systems, today it would be unthinkable to fabricate a patch antenna or an integrated operational amplifier without first carefully vetting the design using CAD tools. Will the development of sophisticated modeling tools for near-field radiative transfer and Casimir phenomena transform those fields as thoroughly as SPICE and its descendants transformed circuit engineering? In the former case, can we use modeling tools to design efficient tip–surface geometries for thermal lithography, or to invent new solar-cell configurations that exploit the interplay of material and geometric properties to optimize power absorption and retention at solar wavelengths? In the latter case, can we use computational tools to understand parasitic Casimir interactions among moving parts in MEMS devices—or to invent new MEMS devices that exploit Casimir forces and torques to useful ends?

All of these are questions for the future of fluctuation-induced phenomena. We hope in this review to have piqued the curiosity of electrical engineers in this rapidly developing field—and to have encouraged readers to stay tuned for future developments.

In closing, we note that all of the computational results presented in this review were obtained using freely-available open-source software packages for computational electromagnetism: MEEP, a finite-difference solver, and SCUFF-EM, a boundary-element solver. (Both packages are available for download at `http://ab-initio.mit.edu/wiki`.) In addition to their general applicability to scattering calculations and other problems in computational electromagnetism, these codes offer specialized modules implementing algorithms discussed in this article for numerical modeling of fluctuation-induced phenomena.

REFERENCES

[1] P. R. Gray, P. J. Hurst, S. H. Lewis, and R. G. Meyer, *Analysis and Design of Analog Integrated Circuits*. Wiley, 2009.

[2] A. I. Volokitin and B. N. J. Persson, "Near-field radiative heat transfer and noncontact friction," *Rev. Mod. Phys.*, vol. 79, pp. 1291–1329, Oct 2007. [Online]. Available: http://link.aps.org/doi/10.1103/RevModPhys. 79.1291

[3] V. Parsegian, *Van der Waals Forces: a Handbook for Biologists, Chemists, Engineers, and Physicists*. Cambridge University Press, 2006.

[4] H. B. G. Casimir, "On the attraction between two perfectly conducting plates," *Koninkl. Ned. Adak. Wetenschap. Proc.*, vol. 51, p. 793, 1948.

[5] T. H. Boyer, "Quantum electromagnetic zero-point energy of a conducting spherical shell and the Casimir model for a charged particle," *Phys. Rev.*, vol. 174, pp. 1764–1776, Oct 1968. [Online]. Available: http://link.aps.org/doi/10.1103/PhysRev.174.1764

[6] M. S. Tomaš, "Casimir force in absorbing multilayers," *Phys. Rev. A*, vol. 66, p. 052103, Nov 2002. [Online]. Available: http://link.aps.org/doi/10.1103/PhysRevA.66.052103

[7] F. Zhou and L. Spruch, "van der Waals and retardation (Casimir) interactions of an electron or an atom with multilayered walls," *Phys. Rev. A*, vol. 52, pp. 297–310, Jul 1995. [Online]. Available: http://link.aps.org/doi/10.1103/PhysRevA.52.297

[8] R. Büscher and T. Emig, "Nonperturbative approach to Casimir interactions in periodic geometries," *Phys. Rev. A*, vol. 69, p. 062101, Jun 2004. [Online]. Available: http://link.aps.org/doi/10.1103/PhysRevA.69.062101

[9] T. Emig, N. Graham, R. L. Jaffe, and M. Kardar, "Casimir forces between arbitrary compact objects," *Phys. Rev. Lett.*, vol. 99, p. 170403, Oct 2007. [Online]. Available: http://link.aps.org/doi/10.1103/PhysRevLett.99.170403

[10] M. T. H. Reid, A. W. Rodriguez, J. White, and S. G. Johnson, "Efficient computation of Casimir interactions between arbitrary 3d objects," *Phys. Rev. Lett.*, vol. 103, p. 040401, Jul 2009. [Online]. Available: http://link.aps.org/doi/10.1103/PhysRevLett.103.040401

[11] M. Levin, A. P. McCauley, A. W. Rodriguez, M. T. H. Reid, and S. G. Johnson, "Casimir repulsion between metallic objects in vacuum," *Phys. Rev. Lett.*, vol. 105, p. 090403, Aug 2010. [Online]. Available: http://link.aps.org/doi/10.1103/PhysRevLett.105.090403

[12] S. Rytov, *Theory of Electric Fluctuations and Thermal Radiation*, ser. AFCRC-TR. Electronics Research Directorate, Air Force Cambridge Research Center, Air Research and Development Command, U.S. Air Force, 1959.

[13] D. Polder and M. Van Hove, "Theory of radiative heat transfer between closely spaced bodies," *Phys. Rev. B*, vol. 4, pp. 3303–3314, Nov 1971. [Online]. Available: http://link.aps.org/doi/10.1103/PhysRevB.4.3303

[14] A. Narayanaswamy and G. Chen, "Thermal near-field radiative transfer between two spheres," *Phys. Rev. B*, vol. 77, p. 075125, Feb 2008. [Online]. Available: http://link.aps.org/doi/10.1103/PhysRevB.77.075125

[15] A. W. Rodriguez, O. Ilic, P. Bermel, I. Celanovic, J. D. Joannopoulos, M. Soljačić, and S. G. Johnson, "Frequency-selective near-field radiative heat transfer between photonic crystal slabs: A computational approach for arbitrary geometries and materials," *Phys. Rev. Lett.*, vol. 107, p. 114302, Sep 2011. [Online]. Available: http://link.aps.org/doi/10.1103/PhysRevLett.107.114302

[16] A. P. McCauley, M. T. Homer Reid, M. Krüger, and S. G. Johnson, "Modeling near-field radiative heat transfer from sharp objects using a general 3d numerical scattering technique," *ArXiv e-prints*, Jul. 2011.

[17] A. W. Rodriguez, F. Capasso, and S. G. Johnson, "The Casimir effect in microstructured geometries," *Nature Photonics*, vol. 5, pp. 211–221, March 2011, invited review.

[18] R. Harrington, *Time-Harmonic Electromagnetic Fields*, ser. IEEE Press series on electromagnétic wave theory. IEEE Press, 1961.

[19] G. L. Klimchitskaya, U. Mohideen, and V. M. Mostepanenko, "Casimir and van der Waals forces between two plates or a sphere (lens) above a plate made of real metals," *Phys. Rev. A*, vol. 61, p. 062107, May 2000. [Online]. Available: http://link.aps.org/doi/10.1103/PhysRevA.61.062107

[20] P. A. Maia Neto, A. Lambrecht, and S. Reynaud, "Casimir energy between a plane and a sphere in electromagnetic vacuum," *Phys. Rev. A*, vol. 78, p. 012115, Jul 2008. [Online]. Available: http://link.aps.org/doi/10.1103/PhysRevA.78.012115

[21] K. A. Milton and J. Wagner, "Exact expressions for the Casimir interaction between semitransparent spheres and cylinders," *Phys. Rev. D*, vol. 77, p. 045005, Feb 2008. [Online]. Available: http://link.aps.org/doi/10.1103/PhysRevD.77.045005

[22] A. Lambrecht, P. A. M. Neto, and S. Reynaud, "The Casimir effect within scattering theory," *New Journal of Physics*, vol. 8, no. 10, p. 243, 2006. [Online]. Available: http://stacks.iop.org/1367-2630/8/i=10/a=243

[23] S. J. Rahi, T. Emig, N. Graham, R. L. Jaffe, and M. Kardar, "Scattering theory approach to electrodynamic Casimir forces," *Phys. Rev. D*, vol. 80, p. 085021, Oct 2009. [Online]. Available: http://link.aps.org/doi/10.1103/PhysRevD.80.085021

[24] S. G. Johnson, "Numerical methods for computing Casimir interactions," *arXiv.org e-Print archive*, July 2010, to appear in upcoming *Lecture Notes in Physics* book on *Casimir Physics*.

[25] H. B. Callen and T. A. Welton, "Irreversibility and generalized noise," *Phys. Rev.*, vol. 83, pp. 34–40, Jul 1951. [Online]. Available: http://link.aps.org/doi/10.1103/PhysRev.83.34

[26] A. Narayanaswamy, S. Shen, and G. Chen, "Near-field radiative heat transfer between a sphere and a substrate," *Phys. Rev. B*, vol. 78, p. 115303, Sep 2008. [Online]. Available: http://link.aps.org/doi/10.1103/PhysRevB.78.115303

[27] M. Krüger, T. Emig, and M. Kardar, "Nonequilibrium electromagnetic fluctuations: Heat transfer and interactions," *Phys. Rev. Lett.*, vol. 106, p. 210404, May 2011. [Online]. Available: http://link.aps.org/doi/10.1103/PhysRevLett.106.210404

[28] G. Bimonte, "Scattering approach to Casimir forces and radiative heat transfer for nanostructured surfaces out of thermal equilibrium," *Phys. Rev. A*, vol. 80, p. 042102, Oct 2009. [Online]. Available: http://link.aps.org/doi/10.1103/PhysRevA.80.042102

[29] C. Otey and S. Fan, "Exact microscopic theory of electromagnetic heat transfer between a dielectric sphere and plate," *ArXiv e-prints*, Mar. 2011.

[30] R. Messina and M. Antezza, "Casimir-Lifshitz force out of thermal equilibrium and heat transfer between arbitrary bodies," *EPL (Europhysics Letters)*, vol. 95, no. 6, p. 61002, 2011. [Online]. Available: http://stacks.iop.org/0295-5075/95/i=6/a=61002

[31] ——, "Scattering-matrix approach to Casimir-Lifshitz force and heat transfer out of thermal equilibrium between arbitrary bodies," *Phys. Rev. A*, vol. 84, p. 042102, Oct 2011. [Online]. Available: http://link.aps.org/doi/10.1103/PhysRevA.84.042102

[32] R. Guérout, J. Lussange, F. S. S. Rosa, J.-P. Hugonin, D. A. R. Dalvit, J.-J. Greffet, A. Lambrecht, and S. Reynaud, "Enhanced radiative heat transfer between nanostructured gold plates," *ArXiv e-prints*, Mar. 2012.

[33] P. Waterman, "Matrix formulation of electromagnetic scattering," *Proceedings of the IEEE*, vol. 53, no. 8, pp. 805 – 812, aug. 1965.

[34] M. Krüger *et al.*, to appear.

[35] M. F. Maghrebi, S. J. Rahi, T. Emig, N. Graham, R. L. Jaffe, and M. Kardar, "Analytical results on Casimir forces for conductors with edges and tips," *Proceedings of the National Academy of Science*, vol. 108, pp. 6867–6871, Apr. 2011.

[36] C. Luo, A. Narayanaswamy, G. Chen, and J. D. Joannopoulos, "Thermal radiation from photonic crystals: A direct calculation," *Physical Review Letters*, vol. 93, pp. 213905–213908, November 2004. [Online]. Available: http://link.aps.org/abstract/PRL/v93/e213905

[37] S. Scheel and S. Yoshi Buhmann, "Macroscopic QED – concepts and applications," *Acta Physica Slovaca*, vol. 58, pp. 675–809, 2008.

[38] H. B. G. Casimir and D. Polder, "The influence of retardation on the London-van der Waals forces," *Phys. Rev.*, vol. 73, pp. 360–372, Feb 1948. [Online]. Available: http://link.aps.org/doi/10.1103/PhysRev.73.360

[39] E. M. L. I. E. Dzyaloshinkii and L. P. Pitaevskii, *Sov. Phys. Usp.*, vol. 4, p. 153, 1961.

[40] E. M. Lifshitz and L. P. Pitaevskii, *Statistical Physics: Part 2*. Pergamon, Oxford, 1980.

[41] H. Gies and K. Klingmüller, "Worldline algorithms for Casimir configurations," *Phys. Rev. D*, vol. 74, p. 045002, Aug 2006. [Online]. Available: http://link.aps.org/doi/10.1103/PhysRevD.74.045002

[42] R. L. Jaffe and A. Scardicchio, "Casimir effect and geometric optics," *Phys. Rev. Lett.*, vol. 92, p. 070402, Feb 2004. [Online]. Available: http://link.aps.org/doi/10.1103/PhysRevLett.92.070402

[43] S. K. Lamoreaux, "Demonstration of the Casimir force in the 0.6 to 6 μm range," *Phys. Rev. Lett.*, vol. 78, pp. 5–8, Jan 1997. [Online]. Available: http://link.aps.org/doi/10.1103/PhysRevLett.78.5

[44] F. Capasso, J. Munday, D. Iannuzzi, and H. Chan, "Casimir forces and quantum electrodynamical torques: Physics and nanomechanics," *Selected Topics in Quantum Electronics, IEEE Journal of*, vol. 13, no. 2, pp. 400 –414, march-april 2007.

[45] L. H. Ford, "Spectrum of the Casimir effect and the Lifshitz theory," *Phys. Rev. A*, vol. 48, pp. 2962–2967, Oct 1993. [Online]. Available: http://link.aps.org/doi/10.1103/PhysRevA.48.2962

[46] A. Rodriguez, M. Ibanescu, D. Iannuzzi, J. D. Joannopoulos, and S. G. Johnson, "Virtual photons in imaginary time: Computing exact Casimir forces via standard numerical electromagnetism techniques," *Phys. Rev. A*, vol. 76, p. 032106, Sep 2007. [Online]. Available: http://link.aps.org/doi/10.1103/PhysRevA.76.032106

[47] S. Weinberg, *The Quantum Theory of Fields, Volume 1*. Cambridge University Press, 1996.

[48] J. D. Jackson, *Classical Electrodynamics*. John Wiley & Sons, 1999.

[49] L. Landau and E. Lifshits, *Electrodynamics of Continuous Media*. Pergamon Press, 1960, no. v. 8.

[50] J.-S. Zhao and W. C. Chew, "Integral equation solution of Maxwell's equations from zero frequency to microwave frequencies," *Antennas and Propagation, IEEE Transactions on*, vol. 48, no. 10, pp. 1635 –1645, oct 2000.

[51] C. L. Epstein and L. Greengard, "Debye sources and the numerical solution of the time harmonic Maxwell equations," *Communications on Pure and Applied Mathematics*, vol. 63, no. 4, pp. 413–463, 2010. [Online]. Available: http://dx.doi.org/10.1002/cpa.20313

[52] A. W. Rodriguez, D. Woolf, A. P. McCauley, F. Capasso, J. D. Joannopoulos, and S. G. Johnson, "Achieving a strongly temperature-dependent Casimir effect," *Phys. Rev. Lett.*, vol. 105, p. 060401, Aug 2010. [Online]. Available: http://link.aps.org/doi/10.1103/PhysRevLett.105.060401

[53] A. O. Shuskov, W. J. Kim, D. A. R. Dalvit, and S. K. Lamoreaux, "Observation of the thermal Casimir force," *Nature Physics*, pp. 230–233, Feb 2011.

[54] C. Genet, A. Lambrecht, and S. Reynaud, "Casimir force and the quantum theory of lossy optical cavities," *Phys. Rev. A*, vol. 67, p. 043811, Apr 2003. [Online]. Available: http://link.aps.org/doi/10.1103/PhysRevA.67.043811

[55] K. A. Milton and J. Wagner, "Multiple scattering methods in Casimir calculations," *Journal of Physics A: Mathematical and Theoretical*, vol. 41, no. 15, p. 155402, 2008. [Online]. Available: http://stacks.iop.org/1751-8121/41/i=15/a=155402

[56] P. A. Maia Neto, A. Lambrecht, and S. Reynaud, "Casimir energy between a plane and a sphere in electromagnetic vacuum," *Phys. Rev. A*, vol. 78, p. 012115, Jul 2008. [Online]. Available: http://link.aps.org/doi/10.1103/PhysRevA.78.012115

[57] P. S. Davids, F. Intravaia, F. S. S. Rosa, and D. A. R. Dalvit, "Modal approach to Casimir forces in periodic structures," *Phys. Rev. A*, vol. 82, p. 062111, Dec 2010. [Online]. Available: http://link.aps.org/doi/10.1103/PhysRevA.82.062111

[58] O. Kenneth and I. Klich, "Casimir forces in a T-operator approach," *Phys. Rev. B*, vol. 78, p. 014103, Jul 2008. [Online]. Available: http://link.aps.org/doi/10.1103/PhysRevB.78.014103

[59] R. Wittmann, "Spherical wave operators and the translation formulas," *Antennas and Propagation, IEEE Transactions on*, vol. 36, no. 8, pp. 1078 –1087, aug 1988.

[60] M. A. Pasquali, S., "Fluctuation-induced interactions between dielectrics in general geometries," *Journal of Chemical Physics*, vol. 129, no. 1, 2008.

[61] A. W. Rodriguez, A. P. McCauley, J. D. Joannopoulos, and S. G. Johnson, "Casimir forces in the time domain: Theory," *Phys. Rev. A*, vol. 80, p. 012115, Jul 2009. [Online]. Available: http://link.aps.org/doi/10.1103/PhysRevA.80.012115

[62] A. P. McCauley, A. W. Rodriguez, J. D. Joannopoulos, and S. G. Johnson, "Casimir forces in the time domain: Applications," *Phys. Rev. A*, vol. 81, p. 012119, Jan 2010. [Online]. Available: http://link.aps.org/doi/10.1103/PhysRevA.81.012119

[63] K. Pan, A. P. McCauley, A. W. Rodriguez, M. T. H. Reid, J. K. White, and S. G. Johnson, "Calculation of nonzero-temperature Casimir forces in the time domain," *Phys. Rev. A*, vol. 83, p. 040503, Apr 2011. [Online]. Available: http://link.aps.org/doi/10.1103/PhysRevA.83.040503

[64] J. L. Xiong and W. C. Chew, "Efficient evaluation of Casimir force in z-invariant geometries by integral equation methods," *Applied Physics Letters*, vol. 95, no. 15, pp. 154 102 –154 102–3, oct 2009.

[65] J. L. Xiong, M. S. Tong, P. Atkins, and W. C. Chew, "Efficient evaluation of Casimir force in arbitrary three-dimensional geometries by integral equation methods," *Physics Letters A*, vol. 374, pp. 2517–2520, May 2010.

[66] M. T. H. Reid, J. White, and S. G. Johnson, "Computation of Casimir interactions between arbitrary three-dimensional objects with arbitrary material properties," *Phys. Rev. A*, vol. 84, p. 010503, Jul 2011. [Online]. Available: http://link.aps.org/doi/10.1103/PhysRevA.84.010503

[67] M. T. H. Reid, "Fluctuating surface currents: A new algorithm for efficient prediction of Casimir interactions among arbitrary materials in arbitrary geometries," Ph.D. dissertation, Massachusetts Institute of Technology, Cambridge, Massachusetts, Feb. 2011.

[68] M. T. H. Reid *et al.*, to appear.

[69] L. N. Medgyesi-Mitschang, J. M. Putnam, and M. B. Gedera, "Generalized method of moments for three-dimensional penetrable scatterers," *J. Opt. Soc. Am. A*, vol. 11, no. 4, pp. 1383–1398, Apr 1994. [Online]. Available: http://josaa.osa.org/abstract.cfm?URI=josaa-11-4-1383

[70] J. N. Munday, F. Capasso, and V. Parsegian, "Measured long-range repulsive Casimir-Lifshitz forces," *Nature (London)*, vol. 457, p. 170, 2009.

[71] A. W. Rodriguez, A. P. McCauley, D. Woolf, F. Capasso, J. D. Joannopoulos, and S. G. Johnson, "Nontouching nanoparticle diclusters bound by repulsive and attractive Casimir forces," *Phys. Rev. Lett.*, vol. 104, p. 160402, Apr 2010. [Online]. Available: http://link.aps.org/doi/10.1103/PhysRevLett.104.160402

[72] L. Greengard and V. Rokhlin, "A fast algorithm for particle simulations," *Journal of Computational Physics*, vol. 73, no. 2, pp. 325 – 348, 1987. [Online]. Available: http://www.sciencedirect.com/science/article/pii/0021999187901409

[73] J. Phillips and J. White, "A precorrected-FFT method for electrostatic analysis of complicated 3-d structures," *Computer-Aided Design of Integrated Circuits and Systems, IEEE Transactions on*, vol. 16, no. 10, pp. 1059 –1072, oct 1997.

[74] X.-C. Nie, L.-W. Li, and N. Yuan, "Precorrected-FFT algorithm for solving combined field integral equations in electromagnetic scattering," in *Antennas and Propagation Society International Symposium, 2002. IEEE*, vol. 3, 2002, pp. 574 – 577 vol.3.

[75] N. Yuan, T. S. Yeo, X.-C. Nie, and L. W. Li, "A fast analysis of scattering and radiation of large microstrip antenna arrays," *Antennas and Propagation, IEEE Transactions on*, vol. 51, no. 9, pp. 2218 – 2226, sept. 2003.

[76] T. Moselhy, X. Hu, and L. Daniel, "PFFT in FastMaxwell: A fast impedance extraction solver for 3d conductor structures over substrate," in *Design, Automation Test in Europe Conference Exhibition, 2007. DATE '07*, april 2007, pp. 1 –6.

M. T. Homer Reid received the B.A. degree in physics from Princeton University in 1998 and the Ph.D. degree in physics from the Massachusetts Institute of Technology (MIT) in 2011. From 1998 to 2003 he was Member of Technical Staff (analog and RF integrated circuit design) at Lucent Technologies Microelectronics and Agere Systems. He is currently a postdoctoral research associate in the Research Laboratory of Electronics at MIT. His research interests include computational methods for classical electromagnetism, fluctuation-induced phenomena, quantum field theory, electronic structure, and quantum chemistry. He is developer and distributor of SCUFF-EM, a free, open-source software package for boundary-element analysis of problems in electromagnetism, including nanophotonics, passive RF component modeling, and Casimir phenomena.

Alejandro W. Rodriguez received a B.S. degree in physics from the Massachusetts Institute of Technology (MIT) in 2006 and a Ph.D. in physics from MIT in 2010. He is currently a joint Postdoctoral Fellow at the Harvard School of Engineering and Applied Sciences and at the MIT Department of Mathematics, working in the areas of computational fluctuation-induced interactions and nanophotonics. Dr. Rodriguez's work comprise some of the earliest numerical methods for Casimir calculations, including the first demonstration of unusual, non-additive, three-body Casimir effects. He is co-author of over 35 publications and 4 patents in the areas of nonlinear nanophotonics, Casimir and optomechanical forces, and non-equilibrium near-field radiative transport. He was named a Department of Energy Computational Science Graduate Fellow from 2006-2010, was the recipient of the 2011 Department of Energy Fredrick Howes Award in Computational Science, and was chosen as a World Economic Forum Global Shaper in 2011. In addition to his research interests, Dr. Rodriguez participates actively in educational initiatives aimed at motivating young students to pursue careers in science and engineering: he was featured in the Spanish-language network Univision, and on the APS Physics central website, as part of educational campaigns to increase the number of graduates and underrepresented minorities in STEM fields, and is currently the professional advisor at the Harvard Society of Mexican American Engineers and Scientists. A native of Cuba, Dr. Rodriguez is an avid salsa dancer, film enthusiast, and Cuban hip hop aficionado.

Steven G. Johnson received B.S degrees in physics, mathematics, and computer science from the Massachusetts Institute of Technology (MIT) in 1995, and a Ph.D. degree in physics from MIT in 2001. Currently, he is Associate Professor of Applied Mathematics at MIT, where he joined the faculty of the Department of Mathematics in 2004. He is active in the field of nanophotonics—electromagnetism in media structured on the wavelength scale, especially in the infrared and optical regimes—where he works on many aspects of the theory, design, and computational modeling of nanophotonic devices. He is co-author of over 150 papers and over 25 patents, including the second edition of the textbook Photonic Crystals: Molding the Flow of Light, and was ranked among the top ten most-cited authors in the field of photonic crystals by ScienceWatch.com in 2008. Since 2007, his work has extended from primarily classical nanophotonics into the modeling of interactions induced by quantum and thermal electromagnetic interactions, and in particular Casimir forces and near-field radiative transport. In addition to traditional publications, he distributes several widely used free-software packages for scientific computation, including the MPB and Meep electromagnetic simulation tools (cited in over 1000 papers to date) and the FFTW fast Fourier transform library (for which he received the 1999 J. H. Wilkinson Prize for Numerical Software).